JACS
JOURNAL OF THE AMERICAN CHEMICAL SOCIETY

Article

pubs.acs.org/JACS

Solvent and H/D Isotope Effects on the Proton Transfer Pathways in Heteroconjugated Hydrogen-Bonded Phenol-Carboxylic Acid Anions Observed by Combined UV−vis and NMR Spectroscopy

Benjamin Koeppe,[†,‡] Jing Guo,[†] Peter M. Tolstoy,*[,†,§] Gleb S. Denisov,[∥] and Hans-Heinrich Limbach*[,†]

[†]Institut für Chemie und Biochemie, Freie Universität Berlin, Takustrasse 3, D-14195 Berlin, Germany

[‡]Max Born Institut für Nichtlineare Optik und Kurzzeitspektroskopie, Max Born Strasse 2A, D-12489 Berlin, Germany

[§]Department of Chemistry, St. Petersburg State University, Universitetskij pr. 26, 198504 St. Petersburg, Russia

[∥]V.A. Fock Institute of Physics, St. Petersburg State University, Ulyanovskaja 1, St.Petersburg State University, Russia

Supporting Information

ABSTRACT: Heteroconjugated hydrogen-bonded anions A···H···X$^-$ of phenols (AH) and carboxylic/inorganic acids (HX) dissolved in CD_2Cl_2 and CDF_3/CDF_2Cl have been studied by combined low-temperature UV−vis and $^1H/^{13}C$ NMR spectroscopy (UVNMR). The systems constitute small molecular models of hydrogen-bonded cofactors in proteins such as the photoactive yellow protein (PYP). Thus, the phenols studied include the PYP cofactor 4-hydroxycinnamic acid methyl thioester, and the more acidic 4-nitrophenol and 2-chloro-4-nitrophenol which mimic electronically excited cofactor states. It is shown that the ^{13}C chemical shifts of the phenolic residues of A···H···X$^-$, referenced to the corresponding values of A···H···A$^-$, constitute excellent probes for the average proton positions. These shifts correlate with those of the H-bonded protons, as well as with the H/D isotope effects on the ^{13}C chemical shifts. A combined analysis of UV−vis and NMR data was employed to elucidate the proton transfer pathways in a qualitative way. Dual absorption bands of the phenolic moiety indicate a double-well situation for the shortest OHO hydrogen bonds studied. Surprisingly, when the solvent polarity is low the carboxylates are protonated whereas the proton shifts toward the phenolic oxygens when the polarity is increased. This finding indicates that because of stronger ion-dipole interactions small anions are stabilized at high solvent polarity and large anions exhibiting delocalized charges at low solvent polarities. It also explains the large acidity difference of phenols and carboxylic acids in water, and the observation that this difference is strongly reduced in the interior of proteins when both partners form mutual hydrogen bonds.

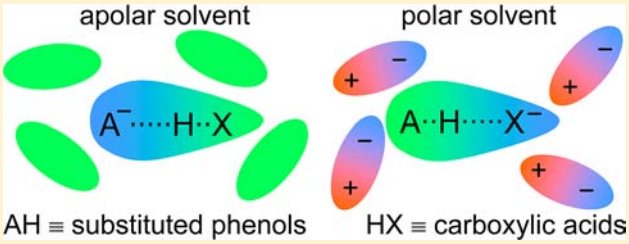

INTRODUCTION

Motivation. Several years ago some of us developed a technique to measure at the same time both low-temperature NMR and UV−vis spectra of a given sample inside an NMR spectrometer (UVNMR).[1] This technique has been applied to study a series of anionic hydrogen-bonded complexes of the type A···H···X$^-$ of 2-chloro-4-nitrophenol AH with acceptors X$^-$ in CD_2Cl_2 solution.[2] That work revealed a qualitative picture of the proton transfer pathway from A$^-$ to X$^-$ and the corresponding changes of NMR and UV−vis spectroscopic observables, most notably a monotonic red shift of optical absorbance of A···H···X$^-$ when H is shifted from A to X. The data also indicated that in the heteroconjugated anion of 2-chloro-4-nitrophenol and benzoic acid both proton donors are similar in acidity, whereas in water the former exhibits a pK_a of 5.45[3] and the latter of 4.2.[4]

The acidity of phenolic residues toward carboxylate residues in the interior of proteins has been an issue debated for quite some time, for example in the case of the active site of photoactive yellow protein (PYP). This protein is a blue light receptor (446 nm) that has been associated with the negative phototactic behavior of some bacteria.[5,6] X-ray and neutron diffraction experiments indicate that its active site bears in the dark state a short and strong or so-called "low-barrier" hydrogen bond between the phenolic oxygen atom of the chromophoric cofactor 4-coumaryl residue[7] and the side chain carboxylic group of Glu46 (Scheme 1).[8−10] However, it is difficult to establish barrier heights of proton transfer in strong hydrogen bonds using diffraction methods. The geometry of this hydrogen bond and thereby charge distribution within the active site are believed to be crucial to the spectral tuning of the photoreceptor. The crystallographic results of Scheme 1 suggest that in the dark state of the protein the cofactor, and to a lesser extend the side chain of the carboxylic group of Glu46, carries a negative charge. Qualitatively, that is in agreement with results of optical spectroscopy. The red-shifted 446 nm absorption maximum of cofactor suggests that it is negatively charged.[8,11,12] In addition, the frequency of the carbonyl

Received: January 18, 2013
Published: April 23, 2013

   dx.doi.org/10.1021/ja400611x | J. Am. Chem. Soc. 2013, 135, 7553−7566

Scheme 1. Schematic Representation of Hydrogen Bonds in Active Site of Photoactive Yellow Protein in the Dark State[a]

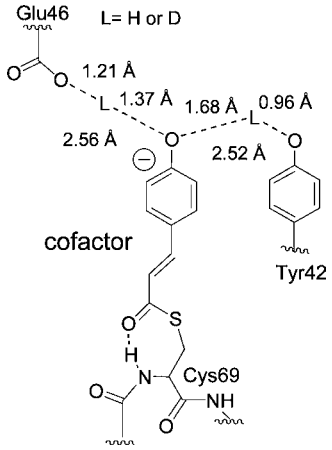

[a]The distances were obtained by a combined analysis of X-ray (L = H) and neutron diffraction data (L = D).[9]

stretching vibration indicates that the side chain carboxylic group of Glu46 is not dissociated.[13]

The question of how exactly the negative charge on the cofactor is stabilized has been a matter of some debate. Localization of the negative charge on the phenolic cofactor instead of on the nearby side chain of Glu46 seems to contradict the relative p$K_a$values of isolated molecular fragments in aqueous solution which are about nine[14] and four,[15] respectively. Thus, it has been argued that as compared to aqueous solution, in the protein the pK_a values change in such a way that the cofactor becomes negatively charged.[16,17] It has been suggested that a positively charged guanidinium group[8,18,19] of the side chain of Arg52 in the proximity of the cofactor has a stabilizing effect on its negative charge. The significance of such an effect could not be verified in the study of a site specific PYP mutant.[18] Moreover, the notion of the existence of positive charge on the side chain of Arg52 in wild-type PYP has also been challenged altogether.[9]

Computational studies suggested that the preferential localization of negative charge on the phenolic cofactor instead of the carboxylic group of Glu46 could be a result of low polarity protein environment.[17] Aspects of cooperativity effects within the hydrogen bond chain have been scrutinized in further studies of site specific PYP mutants.[20]

Aims and Methods. In view of these unsolved questions we thought that it would be useful to extend our previous UVNMR studies of heteroconjugated anions of 2-chloro-4-nitrophenol and to include other phenols (Scheme 2) which are more closely related to the phenolic chromophore in PYP and other proteins. Thus, we choose the 4-coumaric acid thioester (A1H) as phenolic residue to mimic the PYP cofactor hydrogen bonds in the electronic ground state and the more acidic proton donors 4-nitrophenol (A2H) and 2-chloro-4-nitrophenol (A3H) for the more acidic electronically excited states. As proton acceptors we employed mostly carboxylates but in some cases also chloride. Moreover, as we wished to evaluate the influence of the solvent polarity, we choose the polar aprotic media CD_2Cl_2 and CDF_3/CDF_2Cl as solvents. Depending on temperature, these solvents cover a range of dielectric constants of 10 at room temperature to 45 at about 100 K.[21−23] These media model in a better way the hydrophobic environment of protein active sites which are

Scheme 2. Anionic Complexes AHX^- of which UVNMR Studies Are Described in This Work[a]

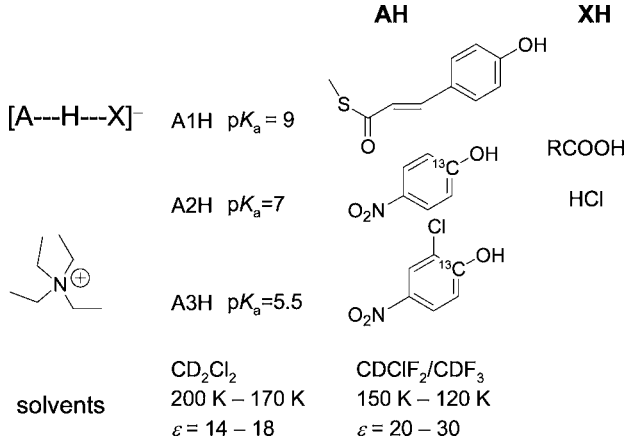

[a]AH represents the proton donors A1H to A3H containing a phenol group, exhibiting different pK_a values as indicated, taken from refs 3, 14, and 51. Anionic proton acceptors X^- are carboxylates or chloride. As counteranion tetraethylammonium was used, as solvents CD_2Cl_2 and the freon mixture CDF_3/CDF_2Cl. The temperature and dielectric constant range covered are indicated.

often shielded from the aqueous phase.[24] The explicit structures of the species studied are depicted in Scheme 3.

In order to estimate average hydrogen bond geometries, previously established spectroscopic correlations, such as NMR hydrogen bond correlations, may be used.[25−27] The most prominent parameter in this context is the chemical shift of the bridging proton, which senses the hydrogen bond compression by a low-field shift.[28−30] In cases of H-bonds formed by carboxylic acids, the NMR parameters of carboxylic carbon have been exploited.[29,31−34] Likewise, in the cases of H-bonds formed by a phenol, the chemical shift of the 1-^{13}C nucleus has been shown to be correlated with H-bond geometry.[2] An especially useful parameter is the H/D isotope effect on chemical shifts.[2,29,32,33,35] For an assessment of the distribution of hydrogen bond geometries rapidly interconverting on the NMR time scale we shall employ combined UV−vis/NMR spectroscopy in order to distinguish between the single and double well proton transfer pathways depicted in Scheme 4, adapted from our previous work.[2] Both pathways involve seven main snapshots or reaction steps, from the non-hydrogen-bonded donor AH not interacting with any acceptor X^- (reaction step 0) to the deprotonated anion A^- not interacting with a proton donor (reaction step ∞). The single well pathway proceeds via a quasi-symmetric reaction step III where the bridging proton takes a central position. By contrast, the double well pathway proceeds via the tautomeric equilibria IIa/b to IVa/b. We note that in case of the single well pathway only a single UV−vis low-energy absorption band will be observed, whereas the double well pathway leads to the appearance of dual bands. This circumstance will be used here in order to distinguish the two reaction pathways and to detect characteristical differences in the corresponding NMR spectra.

This paper is structured as follows. The Experimental Section, describing mainly spectroscopic experiments including the processing of spectral data, is followed by a Results section in which we seek the characterization of hydrogen bond geometries in the model systems studied employing previously established spectroscopic H-bond correlations. In the Dis-

dx.doi.org/10.1021/ja400611x | J. Am. Chem. Soc. 2013, 135, 7553−7566

Scheme 3. Chemical Structures of Anionic Hydrogen-Bonded Complexes AHX^- Studied in This Work

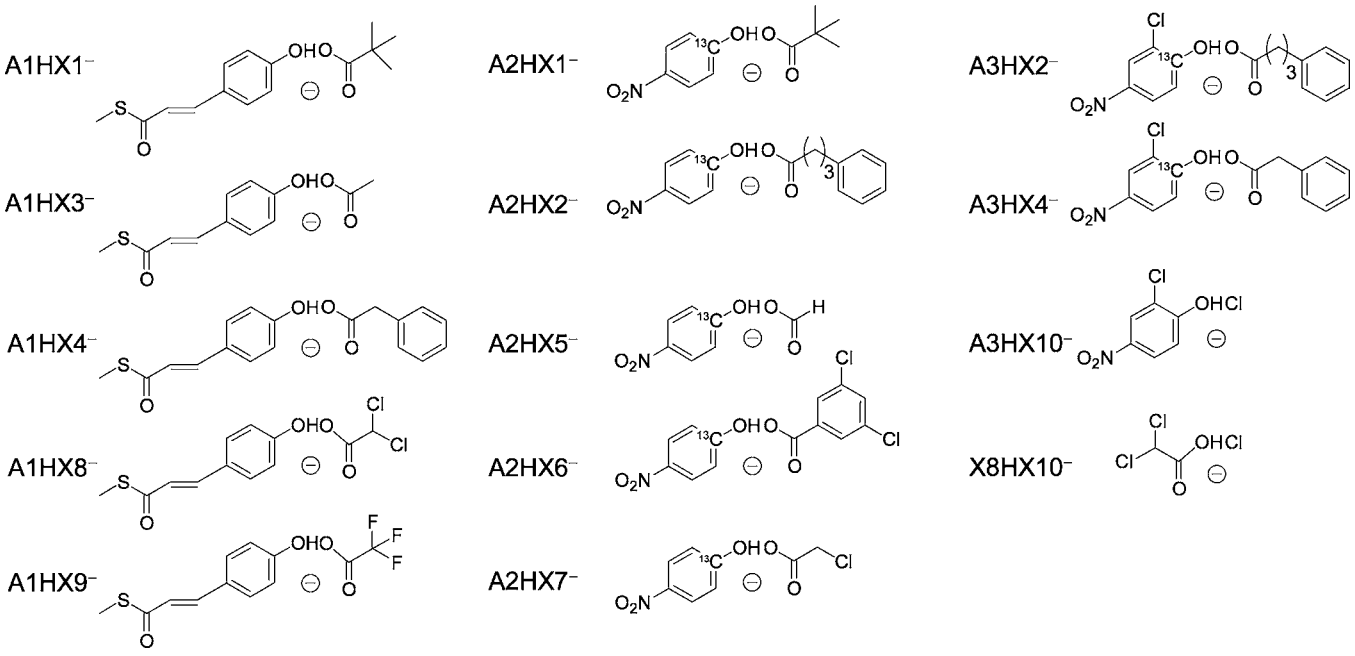

Scheme 4. Schematic Representations of Proton Transfer Pathways: (a) Single Well Pathway Leading through a Very Short Hydrogen Bond Bearing a Single Well Proton Potential and (b) Pathway Involving Equilibria between Two Tautomeric Structures As Proposed Previously[2]

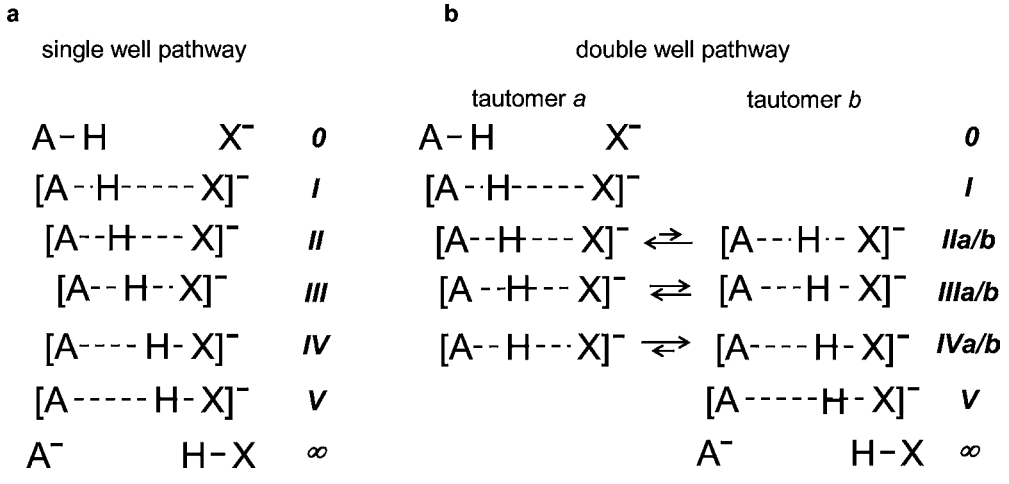

cussion we put the new NMR and UV–vis spectroscopic data in context with existing spectral correlations and concepts of the proton transfer pathway. Then we will particularly discuss the origin of medium effects on hydrogen bond geometry in phenol-carboxylate complexes. Finally, we shall discuss what conclusions we may draw from our findings on model systems in respect to photoactive yellow protein.

EXPERIMENTAL SECTION

Nomenclature. In this paper, we abbreviate phenolic chromophores as AH (specifically defined as A1H, A2H, and A3H in Scheme 2) and their conjugated anionic bases as A^-. Hydrogen bond partners (carboxylic acids, phenols, hydrogen chloride) and their conjugated bases are denoted XH and X^-, respectively. AHX^- then represent the heteroconjugated anions formed by AH and XH as illustrated in Scheme 3.

Syntheses, Sample Preparation, Spectroscopic Experiments. Experimental procedures very similar to those described previously[1,2,32−34] are detailed in the Supporting Information. The key step in the determination of UV–vis absorption spectra of (i) complexes AHX^- and (ii) non-hydrogen bonded A^- with tetraethylammonium (TEA^+) as countercation is the preparation of sample solutions containing target species in the absence of other species absorbing in similar UV–vis spectral ranges. In good approximation exclusive presence of either AHX^- or A^- and absence of other chromophore containing complexes, such as homoconjugated anions AHA^-, can be achieved by appropriate choice of nominal concentrations of HA, TEA^+X^- and HX. As complex equilibria depend on the nature of HA, HX, and the medium, concentration ratios for each system are empirically optimized under NMR guidance.[1,2]

RESULTS

In the following we describe the results of our UVNMR studies of the hydrogen-bonded anions AHX^- of Scheme 3. All spectral parameters obtained are listed in Tables S1 to S4 of the Supporting Information.

dx.doi.org/10.1021/ja400611x | J. Am. Chem. Soc. 2013, 135, 7553−7566

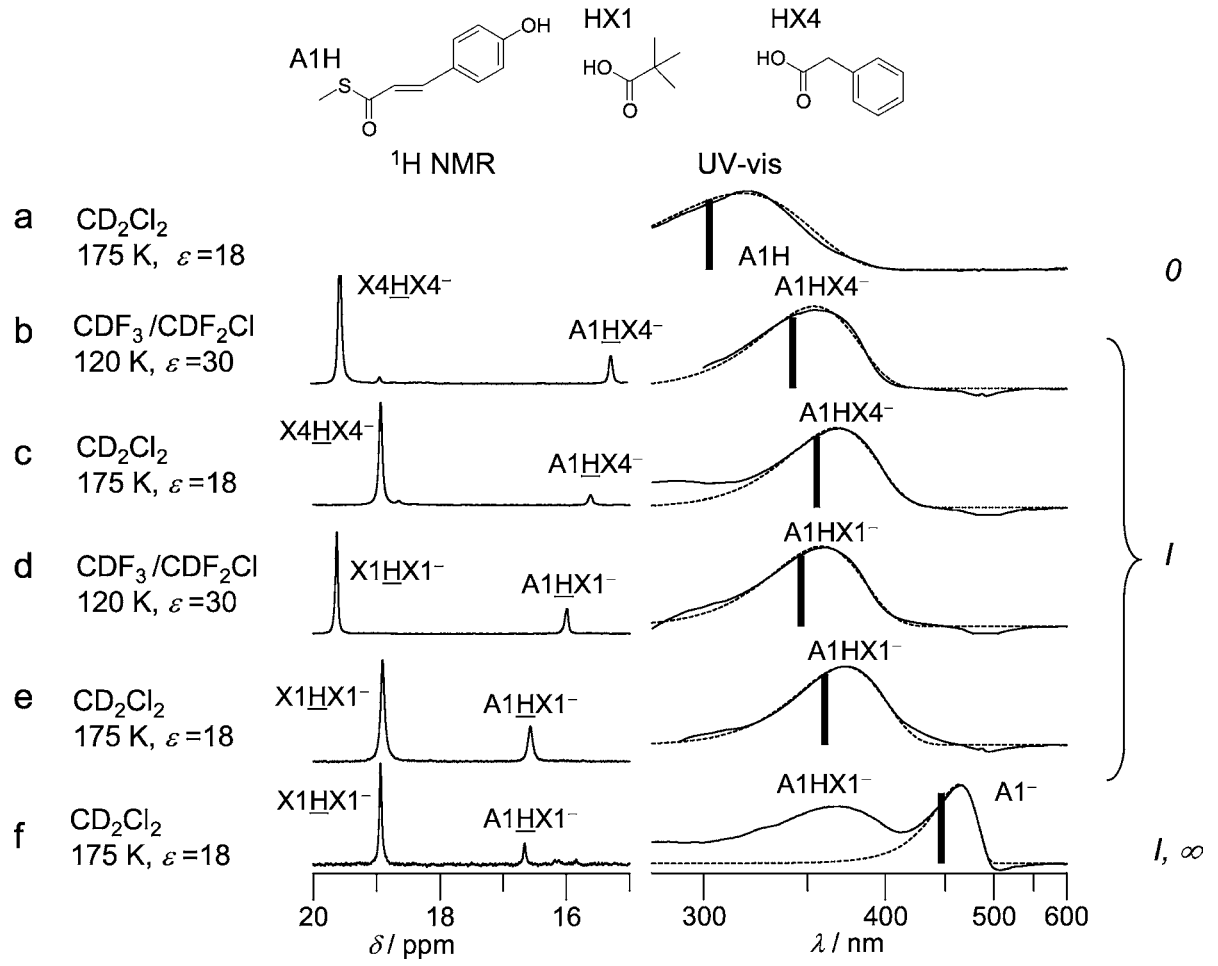

Figure 1. ^{1}H NMR and normalized UV–vis absorption spectra of samples containing heteroconjugated anions A1HX$^-$ of 4-coumaric acid thioester A1H in either CD_2Cl_2 around 175 K or CDF_3/CDF_2Cl at 120 K as solvents. Optical spectra of the limiting cases of the thioester A1H and a sample containing a fraction of its "free" (non-hydrogen-bonded) phenolate form A1$^-$ have been added. Vertical bars in optical spectra indicate centers of gravity of log-normal fit functions (dashed lines). Italics characterize hydrogen bonds in terms of stages on the proton transfer pathway according to Scheme 4. Values for dielectric constants ε for the CDF_3/CDF_2Cl and for CD_2Cl_2 are estimates based on data which have been published previously.[21,23]

Complexes of the 4-Coumaric Acid Thioester A1H. *Spectra.* Some typical ^{1}H NMR spectra and simultaneously recorded UV–vis absorption spectra of solutions containing anionic H-bonded complexes A1HX$^-$ are depicted in Figure 1, together with the corresponding spectra of A1H and its conjugated anion A1$^-$. The experimental UV–vis spectra are represented by solid lines and the simulated spectra by dashed lines. Spectral parameters of all species are collected in Table S1.

In Figure 1a the optical spectrum of A1H in CD_2Cl_2 solution at 175 K is depicted. The experimental band whose maximum is at 319 nm could be fitted with a log-normal function equation of skewness 1.4 with center of gravity at 33 080 cm^{-1} as indicated by the vertical bar. The solubility of A1H in CD_2Cl_2 at low temperatures is considerably below 1 mM and no satisfactory ^{1}H NMR spectra could be obtained. In CDF_3/CDF_2Cl the solubility was even lower and neither type of spectra of A1H could be obtained.

Figure 1b,c depicts the spectra of A1HX4$^-$ and Figure 1d,e those of A1HX1$^-$ in CD_2Cl_2 and CDF_3/CDF_2Cl in the presence of an excess of the homoconjugated anions XHX$^-$ and carboxylates X$^-$. The signals at around 19 ppm are characteristic for X<u>H</u>X$^-$,[2,27] where the resonating H atom is underlined. Signals observed in the 15–17 ppm range are assigned to the heteroconjugated anions. Optical absorption bands with maxima at 360–370 nm are also attributable to these species as the carboxylic acids absorb only below 300 nm. The bands observed have in good approximation a log-normal shape, where the band widths decrease with the absorption frequency as illustrated in Table S1.

For comparison, Figure 1f shows the spectra of a CD_2Cl_2 solution of A1H containing an excess of pivalate X1$^-$. Under these conditions, we observe X1HX1$^-$, some amount of A1HX1$^-$ both by ^{1}H NMR and UV–vis, and in the 430–480 nm region of the optical spectrum the non-hydrogen-bonded anion A1. Its contribution to the optical spectrum may well be described by a narrow log-normal shape. In a similar experiment using CDF_3/CDF_2Cl as solvent no band corresponding to A1$^-$ could be found; this is presumably due to solubility issues. In the 480–550 nm region of the spectra in Figure 1b–f, we observe a small "negative absorbance" which we attributed to the fluorescence of the coumaryl moiety.[38]

For species A1HX8$^-$ and A1HX9$^-$ in CD_2Cl_2 solution chemical shifts of the bridging proton of 13.3 and 12.6 ppm, absorption bands at 350 and 340 nm have been found,

dx.doi.org/10.1021/ja400611x | J. Am. Chem. Soc. 2013, 135, 7553–7566

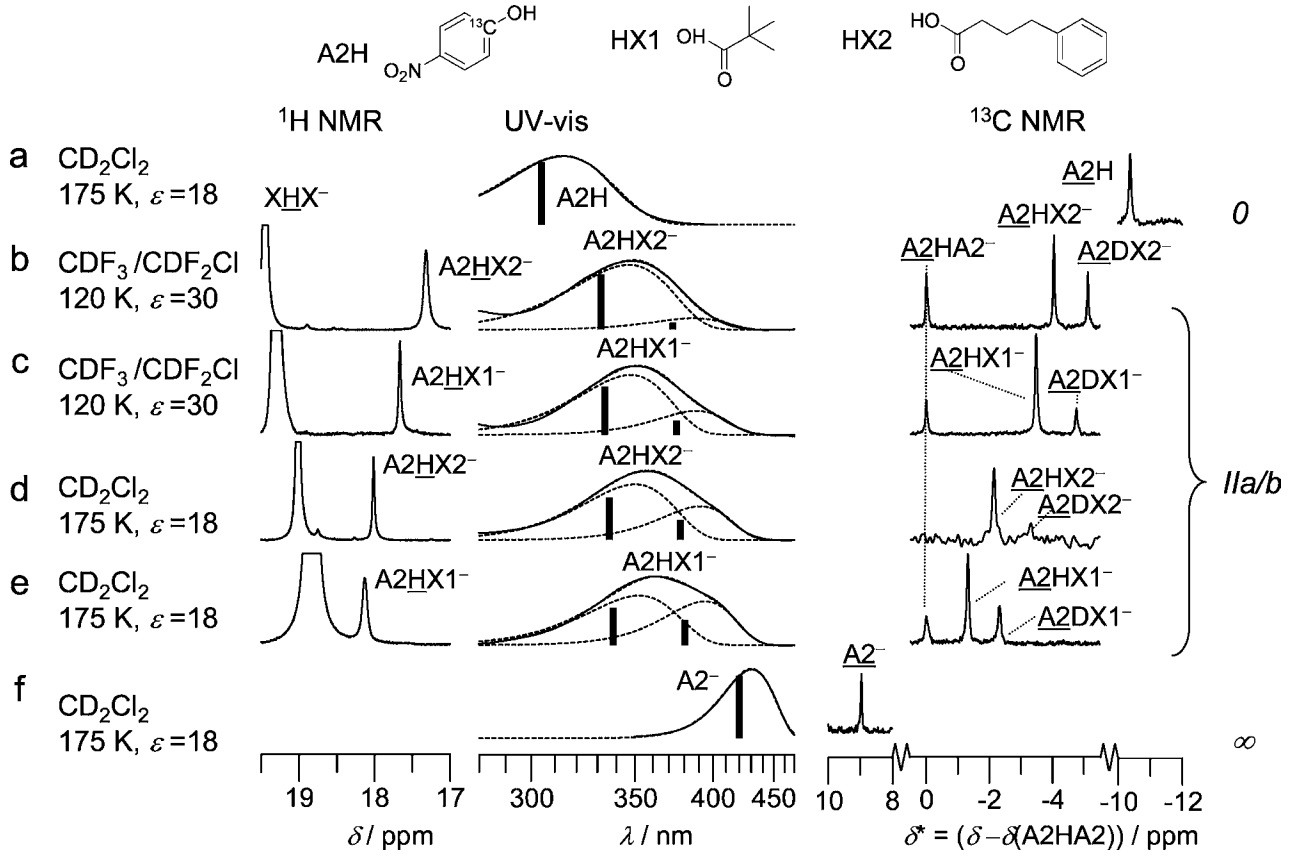

Figure 2. ^{1}H, ^{13}C NMR, and normalized UV−vis absorption spectra of samples containing heteroconjugated anions A2HX⁻ of 1-^{13}C-4-nitrophenol (A2H) in CD_2Cl_2 at 175 K or CDF_3/CDF_2Cl at 120 K. Optical and ^{13}C NMR spectra of the limiting cases of 1-^{13}C-4-nitrophenol (A2H) and 1-^{13}C-4-nitrophenolate (A2⁻) in CD_2Cl_2 have been added. Vertical bars in optical spectra indicate centers of gravity of log-normal fit functions (dashed lines). The ^{13}C NMR spectra are referenced to the 1-^{13}C resonances of the corresponding homoconjugated anions of 4-nitrophenol (A2HA2⁻). Italics characterize hydrogen bonds in terms of stages on the proton transfer pathway according to Scheme 4b.

respectively. The spectra are depicted in the Supporting Information, and the spectral parameters in Table S1.

Spectral Parameters and H-Bond Geometries. The ^{1}H chemical shifts are in the range between 15.3 and 16.6 ppm indicating the presence of medium to short, but not very short, hydrogen bonds. As corroborated later, we assume that H is located closer to the phenolic than to the carboxylate moiety. The shift of the H-bond proton signal to lower field when going from A1HX1⁻ to A1HX4⁻, indicates then a lengthening of the phenolic OH-bond and a shortening of the H···O bond. This is in agreement with the larger basicity of pivalate X1⁻ (pK_a 5.01)[36] as compared to phenylacetate X4⁻ (pK_a 4.31).[3] We note that replacement of CD_2Cl_2 by the more polar CDF_3/CDF_2Cl leads to a lengthening of the hydrogen bonds and small proton displacements toward the phenolic oxygen. This indicates that the hydrogen bond geometries of A1HX1⁻ and A1HX4⁻ correspond to the stages I−II in Scheme 4a.

This interpretation is corroborated by the optical spectra if we assume a similarity in the spectral behavior of chromophore unit A1⁻ to that of A3⁻ studied previously.[2] It was found for the latter that the red shift of the lowest electronic transition of phenols upon deprotonation is occurring predominantly in the early stages of the proton transfer.

Moreover, the optical spectra allow us also to distinguish between single well and double well hydrogen bonds (Scheme 4). For example the transition between type I and IIa/b is manifested by a characteristic broadening of the red shifting absorption bands.[2] In the present cases, the red absorbance shifts are accompanied by narrowing of the bands which is characteristic for species with H-bonds of type I. We note that the red shifts of the optical bands in Figure 1 do not exactly match the findings by ^{1}H NMR, a topic which will be discussed later.

Complexes of 4-Nitrophenol A2H. *Spectra.* Figure 2 shows the combined ^{1}H NMR and UV−vis spectra of solutions of A2H in CD_2Cl_2 and in CDF_3/CDF_2Cl in the presence of anions. In addition, the figure includes separately measured ^{13}C NMR spectra of the 4-nitrophenyl moiety A2⁻ as chromophore. A2H was labeled with ^{13}C in the carbon-1 position in order to obtain easily ^{13}C NMR spectra and H/D isotope effects on the 1-^{13}C resonances. As acids HX1 (pivalic acid, pK_a 5.01) and HX2 (4-phenyl-butyric acid, pK_a 4.76) were used (see Table S3). Absorption bands of A2H and A2⁻ reaching maxima at 314 and 431 nm, respectively, exhibit log-normal shape. In order to eliminate structural influences and highlight the influence of hydrogen bonding, the ^{13}C NMR spectra are referenced to the signal of 1-^{13}C of the corresponding homoconjugated anion AHA⁻ as internal standard, i.e.

$$\delta^*(\underline{A}HX) = \delta(\underline{A}HX) - \delta(\underline{A}HA) \quad (1)$$

leading to chemical shifts of −10.38 and 8.95 ppm for A2H and A2⁻, respectively. This type of referencing will be discussed below.

The ^{1}H NMR spectra contain again signals of the homoconjugated anions XHX⁻ in the range between 18.5 to 20 ppm. The signals in the range between 17.3 and 18.1 ppm

dx.doi.org/10.1021/ja400611x | J. Am. Chem. Soc. 2013, 135, 7553−7566

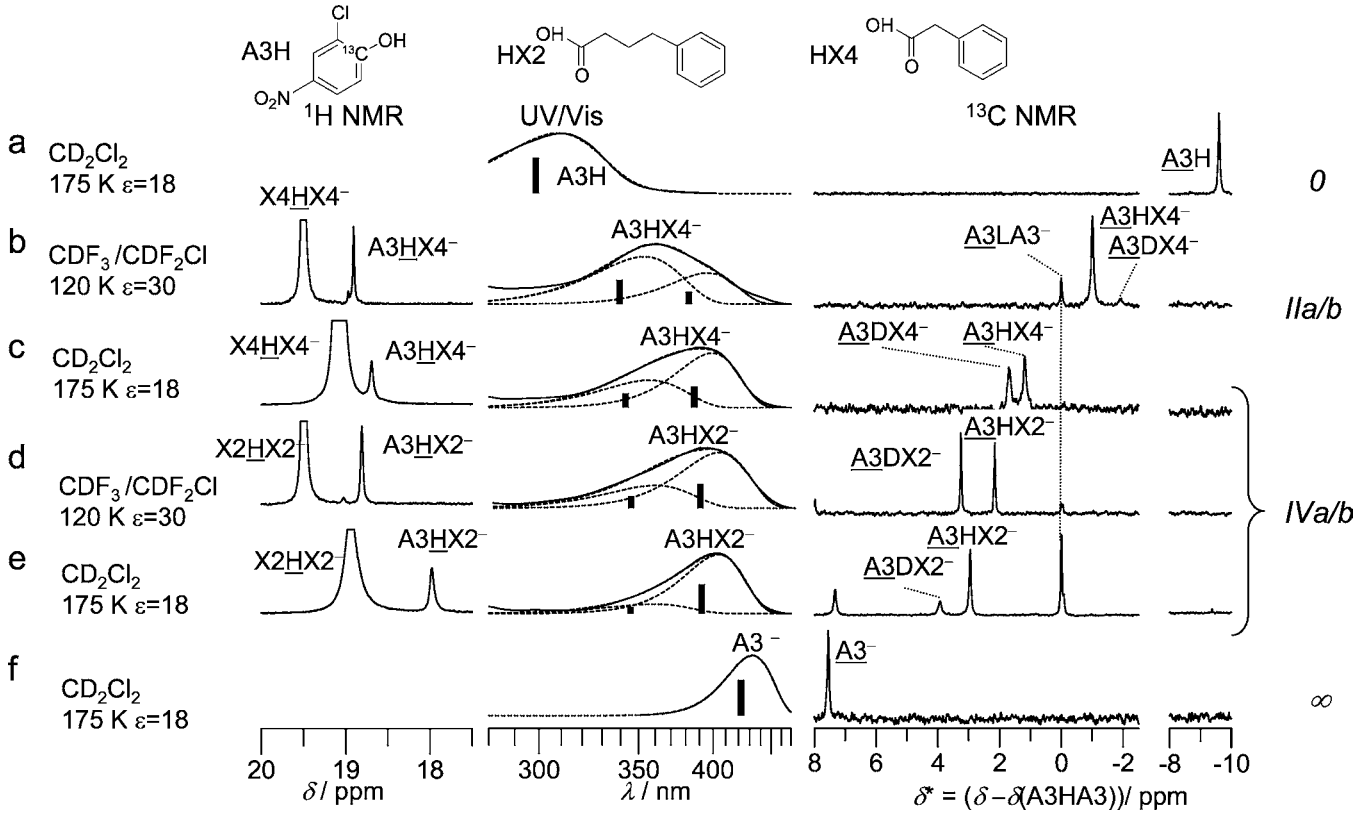

Figure 3. ^{1}H, ^{13}C NMR, and normalized UV−vis absorption spectra of samples containing heteroconjugated anions ($A3HX^-$) of 1-^{13}C-2-chloro-4-nitrophenol (A3H) in CD_2Cl_2 at 175 K or Freons at 120 K. Optical and ^{13}C NMR spectra of the limiting cases of the phenol (A3H) and the phenolate $A3^-$ in CD_2Cl_2 solution have been added. Vertical bars in optical spectra indicate centers of gravity of log-normal fit functions (dashed lines). ^{13}C NMR spectra are given calibrated to 0 ppm for the 1-^{13}C resonance of homoconjugated anion $A3HA3^-$ of the phenol. Italics characterize hydrogen bonds in terms of stages on the proton transfer pathway according Scheme 4b.

arise from the heteroconjugated anions $A2\underline{H}X^-$. They exhibit a monotonous downfield shift when the basicity or the solvent polarity is increased. In the same order, the 1-^{13}C resonance of the phenol moiety of $A2HX^-$ is shifted to low field. Moreover, secondary H/D isotope effects Δ on 1-^{13}C chemical shifts are observed,

$$\Delta = \delta(\underline{A}DX) - \delta(\underline{A}HX) \quad (2)$$

which are all negative.

The samples were prepared in such a way that the heteroconjugated anions $A2HX^-$ dominate the optical spectra.[1,2] Within the given order, absorption bands of $A2HX^-$ shift red in the range between 350 and 360 nm and broaden (from 4900 to 5600 cm^{-1}). Parameters of ^{1}H NMR and optical spectra are collected in Table S1 and parameters of ^{13}C NMR spectra are collected in Table S2.

Spectral Parameters and H-Bond Geometries. Proton chemical shifts exceeding 17 ppm indicate that the anions $A2HX1^-$ and $A2HX2^-$ exhibit shorter hydrogen bonds than the coumaryl ester anions $A1HX^-$ of the previous section. Average proton positions can be qualitatively inferred from the ^{13}C NMR spectra as it has been established that the downfield shift of a phenolic 1-^{13}C signal in AHX^- from the one of AHA^- indicates that H is located on average closer to X than to A, whereas the contrary is true for a high-field shift.[2] Thus, for the spectra of Figure 2, we conclude that H is located closer to the 4-nitrophenol moiety $A2^-$, but is monotonously displaced on average toward the hydrogen bond center when the solvent polarity or the basicity of the acid residue is decreased. This corresponds to the stages I to II in Scheme 4a. However, it is difficult to distinguish single and double-well situations.

A look at the UV−vis spectra of Figure 2b−e shows a considerable broadening of the bands of $A2HX^-$ when H is shifted on average toward the hydrogen bond center, which is consistent with dual absorption bands corresponding to asymmetric double wells or tautomeric states IIa/b in Scheme 4b. The spectra were, therefore, decomposed into dual bands according to a procedure established previously.[2] Individual contributions as well as their sum are illustrated by dashed lines while vertical bars indicate individual centers of gravity. The monotonous trend within the four spectra extends to the individual components: both "blue bands" and "red bands" shift red within the series while the blue band loses intensity with respect to the red band.

To summarize, A2H is a stronger acid than the 4-coumaric acid thioester A1H. In species $A2HX2^-$ and $A2HX1^-$ bridging protons are displaced from the phenolic oxygen atom toward the hydrogen bond center following the order of basicities $X1^- > X2^-$. Interestingly, for both species this displacement is smaller when the solvent polarity is increased.

Complexes of 2-Chloro-4-nitrophenol A3H. *Spectra.* Finally, we have measured spectra of solutions of A3H which is the most acidic phenol in Scheme 2, in the presence of the anions of the acids HX2 (4-phenyl-butyric acid) and HX4 (phenylacetic acid). The UV−vis and ^{13}C NMR spectra of pure A3H and $A3^-$ in CD_2Cl_2, depicted in Figure 3a,f, were taken from ref 2. The optical spectrum of A3H in CDF_3/CDF_2Cl, shown in Figure 1 of the Supporting Information and

dx.doi.org/10.1021/ja400611x | J. Am. Chem. Soc. 2013, 135, 7553−7566

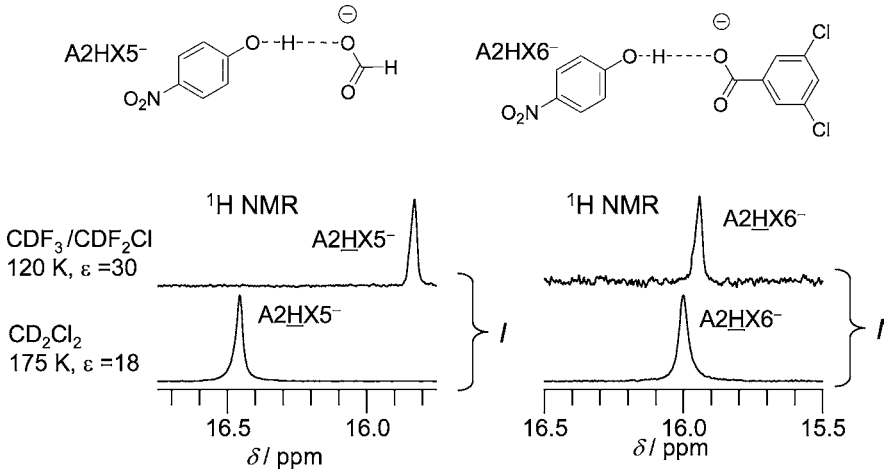

Figure 4. ^{1}H NMR spectra of samples containing the heteroconjugated anions of 4-nitrophenol with formic acid A2HX5^{-} (left) and 3,5-dichlorobenzoic acid A2HX6^{-} (right). Upper and lower spectra were recorded in CDF_3/CDF_2Cl solution at 120 K and CD_2Cl_2 solution at 175 K, respectively. Italics characterize hydrogen bonds in terms of stages on the proton transfer pathway according to Scheme 4.

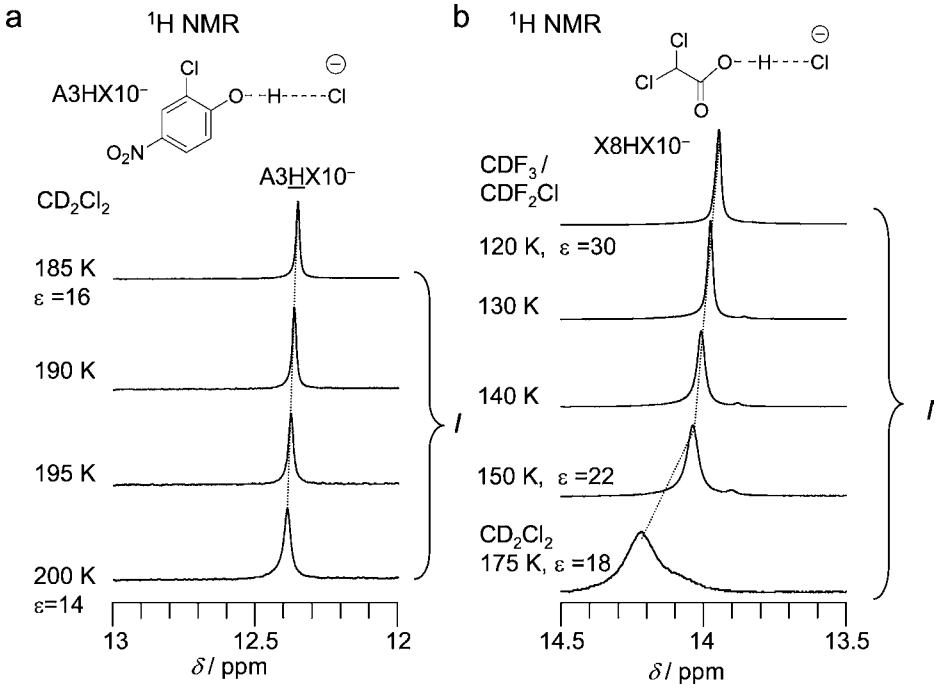

Figure 5. ^{1}H NMR spectra of samples containing (a) the complex A3HX10^{-} of chloride with 2-chloro-4-nitrophenol obtained in CD_2Cl_2 solution at various temperatures and (b) the complex X8HX10^{-} of chloride with dichloroacetic acid measured in CDF_3/CDF_2Cl solution at various temperatures between 120 and 150 K and in CD_2Cl_2 solution at 175 K. Hydrogen bonds are characterized as stage *I* in terms of the proton transfer pathway in Scheme 4.

summarized in Table S1, is very similar to that obtained for CD_2Cl_2.

As can be seen in Figure 3, the signals of the homoconjugated anions XHX^{-} dominate in the ^{1}H NMR spectra. The minor signals in the 18−19 ppm range arise from the heteroconjugated anions A3HX^{-} and indicate the presence of strong hydrogen bonds. These species give rise to UV−vis absorption bands that monotonously shift red beginning from 363 nm for A3HX4^{-} in CDF_3/CDF_2Cl (Figure 3b) to 402 nm for A3HX2^{-} in CD_2Cl_2 (Figure 3e). Within the same order, the 1-^{13}C signals of the phenol moieties of A3HX^{-} shift downfield, custom referenced chemical shifts δ^* increase from −1.0 to 2.9 ppm.

Spectral Parameters and H-Bond Geometries. As before, the NMR signals of 1-^{13}C of the phenol allow us to estimate the average proton positions. We find the chemical shift δ^* to be negative for A3HX4^{-} in the spectrum in Figure 3b, but increasingly positive values are observed in the spectra of Figure 3c−e. Interestingly, in the same series the secondary H/D isotope effect is first negative, changes sign, and increases monotonously. Thus, the ^{13}C NMR data suggest a progressive displacement of the average proton position from the phenolic oxygen through the hydrogen bond center toward the carboxylic group. The effect occurs when the solvent polarity is decreased and/or the more basic acid residue is present.

This interpretation is supported by the monotonous red shift of UV−vis absorption bands which have been discussed

dx.doi.org/10.1021/ja400611x | J. Am. Chem. Soc. 2013, 135, 7553−7566

previously[2] for A3HX4$^-$ in CD_2Cl_2 solution. We observe again dual absorption bands as illustrated by the dashed lines, where both the "blue bands" and "red bands" shift red within the series. These results indicate an asymmetric double well situation according to Scheme 4b. Whereas in CDF_3/CDF_2Cl A3HX4$^-$ adopts stage IIa/b where the tautomer IIa with H closer to the phenolic moiety dominates, A3HX4$^-$ adopts stage IVa/b in the less polar solvent CD_2Cl_2 where the tautomer IVb with H closer to the carboxylic oxygen dominates. By contrast, A3HX2$^-$ adopts this stage already in CDF_3/CDF_2Cl as the acid residue is more basic than in A3HX4$^-$.

To summarize this section, we again find that a decrease of the solvent polarity promotes proton transfer toward the carboxylic group.

Effects of the Acid Size and the Solvent Polarity on the Geometries of Heteroconjugated Hydrogen-Bonded Anions. In order to elucidate a possible relationship between the solvent polarity induced basicity changes in acid residues and their volume (or "effective size") we carried out the NMR experiments described in this section. In Figure 4 we compare the ^{1}H NMR spectra of the heteroconjugated anions A2HX5$^-$ and A2HX6$^-$ of 4-nitrophenol with the small formate and the large 3,5-dichlorobenzoate, dissolved in the very polar CDF_3/CDF_2Cl at 120 K as well as in the less polar CD_2Cl_2 at 175 K. All four systems are of the type I, as both formate and 3,5-dichlorobenzoate are considerably weaker bases than pivalate and 4-phenylacetate,[2] whose complexes with 4-nitrophenol were described above as of type II.

In CDF_3/CDF_2Cl the bridging protons of both A2HX5$^-$ and A2HX6$^-$ display similar chemical shifts of 15.8 and 15.9 ppm, respectively, corresponding to quite similar hydrogen bond geometries. When A2HX5$^-$ is studied in CD_2Cl_2 the proton signal shifts by 0.7 ppm to almost 16.5 ppm, indicating a contraction of the hydrogen bond and a proton displacement toward the carboxylate. However, the corresponding chemical shift in A2HX6 is increased only by less than 0.1 ppm when CDF_3/CDF_2Cl is replaced by CD_2Cl_2, indicating that in this case the effect of the solvent polarity on hydrogen geometry is very small.

In order to strengthen these findings further, we have studied heteroconjugated anions of the much smaller chloride with the large 2-chloro-4-nitrophenol and dichloroacetic acid, leading to the species A3HX10$^-$ and X8HX10$^-$. Their ^{1}H NMR spectra in CDF_3/CDF_2Cl and CD_2Cl_2 recorded at various temperatures are depicted in Figure 5.

The hydrogen-bonded protons resonate in the 12 to 14.5 ppm range, indicating rather long hydrogen bonds. As chloride is a very weak base, H is located closer to the oxygen atoms and farer away from chloride. Figure 5a indicates that the signal of the bridging proton in A3HX10$^-$ is only slightly shifted by 0.04 ppm to lower field when temperature is increased from 185 to 200 K. According to Figure 5b, for X8HX10$^-$ in CDF_3/CDF_2Cl a similar downfield shift from 13.95 to 14.04 ppm is observed when temperature is increased from 120 to 150 K. However, a stronger downfield shift (14.22 ppm) is found for the anion in CD_2Cl_2 solution at 175 K.

As small as these temperature effects are, they seem nevertheless significant in terms of indicating a shortening of the Cl...H hydrogen bond distance when temperature increases. We note that these shifts cannot arise from proton exchange with residual water when temperature is increased, as in this case a high-field shift would be observed. Therefore, we associate the observed Cl···H distance decrease to the decrease of the dielectric constants with increasing temperature[21,23] included in Figure 5.

DISCUSSION

We have studied the hydrogen-bonded complexes of the 4-coumaric acid thioester A1H and of the two more acidic phenols A2H and A3H with carboxylates X$^-$ in aprotic solvents. The chemical structures of the heteroconjugated anions formed, AHX$^-$, were depicted in Schemes 2 and 3. These anions may be regarded as simple models for the hydrogen-bonded coumarin cofactor and Glu46 in PYP (Scheme 1). Whereas A1HX$^-$ is the most appropriate model for the electronic ground state of the cofactor under various conditions, A2HX$^-$ and A3HX$^-$ might be used as models for the electronically excited state in which the acidity of the cofactor has increased. By UVNMR we observed two types of samples of AHX$^-$ in organic polar solvent, one type exhibiting single and the other dual UV−vis absorption bands. Whereas the first type indicates the presence of single tautomers, the second one is typical for a tautomeric equilibrium. Strong effects of the polarity of the medium on the hydrogen bond geometries are observed.

The main part of this section is devoted to the analysis of the spectroscopic data obtained and their correlation with the corresponding hydrogen bond geometries from which details of the reaction pathways of proton transfer result. We will then discuss the influence of the medium polarity on the H-bond geometries of AHX$^-$, i.e., on the acid−base behavior of the partners. Finally, we will consider the biological implications of our findings.

Proton Transfer Pathways from Combined ^{1}H NMR and UV−vis Spectroscopy. It has been shown previously that the distances r_{AH} and r_{HX} of hydrogen-bonded systems of the type AHX are correlated with each other.[37] Therefore, also the hydrogen bond coordinates

$$q_1 = {}^1/_2(r_{AH} - r_{HX}) \text{ and } q_2 = r_{AH} + r_{HX} \quad (3)$$

are correlated with each other.[28] q_1 represents the distance of the proton from the hydrogen bond center and q_2 the A···X distance. In the absence of a proton tautomerism, for OHO hydrogen bonds, q_1 can be estimated from the ^{1}H chemical shifts using the following equation[28]

$$\delta(\underline{\text{AH}}\text{X}) = \delta(\underline{\text{AH}})^\circ + \Delta(\underline{\text{AH}}\text{X}) \exp(-6.2q_1^2) \quad (4)$$

$\delta(\underline{\text{AH}})^\circ$ represents the chemical shift of the fictive free non-hydrogen-bonded OH group, and $\Delta(\underline{\text{AH}}\text{X})$ the excess low-field shift upon formation of the strongest OHO hydrogen bond exhibiting an O···O distance of about 2.4 Å. Equation 4 represents an approximation to a more general formalism.[28] In particular, eq 4 neglects the chemical shift difference of isolated phenols and carboxylic acids. For example DFT calculations give $\delta(\underline{\text{AH}})^\circ \approx 6$ ppm for formic acid and 3 ppm for phenol.[28] Here we used an average value of 4 ppm in eq 4, and the value of $\Delta = 16.5$ ppm, leading to a maximum chemical shift of 20.5 ppm for the shortest OHO hydrogen bond. Figure 6a shows a graph of $\delta(\underline{\text{AH}}\text{X})$ as a function of q_1, where eq 4 is represented by the solid line. In the next step, we used the experimental ^{1}H chemical shifts of the anions AHX$^-$ exhibiting single UV−vis bands to estimate the corresponding q_1 values using eq 4. The resulting data points are then perfectly located on the solid curve as illustrated in Figure 6a. Then we calculated the

dx.doi.org/10.1021/ja400611x | J. Am. Chem. Soc. 2013, 135, 7553−7566

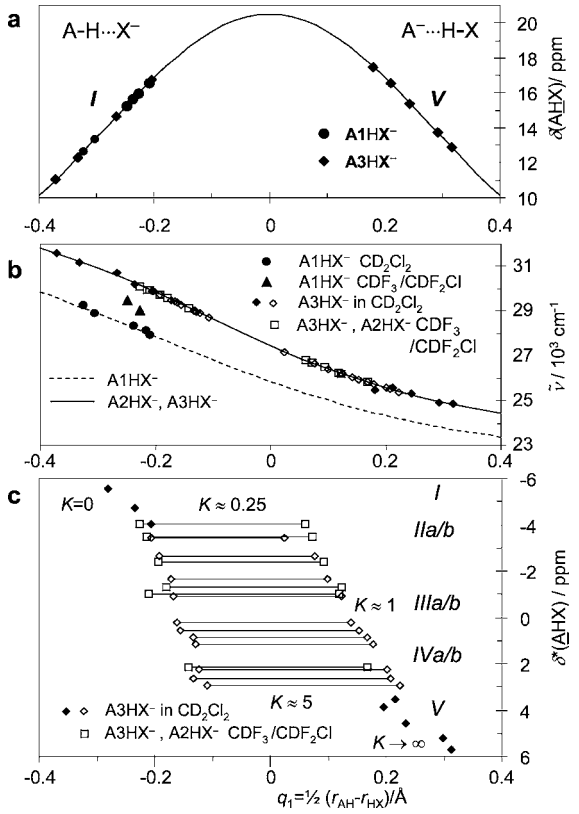

Figure 6. Correlations between spectral parameters and the proton coordinate $q_1 = {}^1/_2(r_{AH} - r_{HX})$ of complexes AHX^- in the aprotic polar solvents CD_2Cl_2 and CDF_3/CDF_2Cl. (a) Experimental proton chemical shifts $\delta(A\underline{H}X)$ as a function of q_1. (b) Experimental electronic transition energies (as $\tilde{\nu}_{COG}$) as a function of q_1. (c) Estimated q_1 values of single well configurations and of tautomeric states of AHX^-, separated by the ^{13}C chemical shifts $\delta^*(\underline{A}HX) = \delta(\underline{A}HX) - \delta(\underline{A}HA)$ of the phenolic carbon atoms 1-^{13}C of AHX^-, referenced to those of AHA^-. For further explanations see text.

corresponding values of q_2 as described previously.[28] The data obtained are included in Table S1.

In Figure 6b we have plotted the observed UV band wavenumbers as a function of the estimated q_1 values, represented by the solid symbols. The latter could well be described by the solid correlation curve calculated using the empirical eq 5 derived previously[2] for 2-chloro-4-nitrophenol $A3HX^-$ complexes in CD_2Cl_2

$$\tilde{\nu}_{AHX} = \tilde{\nu}_A + (\tilde{\nu}_{AH} - \tilde{\nu}_A)/\left(1 + \exp\frac{q_1 + a}{b}\right) \quad (5)$$

$\tilde{\nu}_{AH}$ and $\tilde{\nu}_A$ principally correspond to the center of gravity of the absorption bands of monomeric phenol AH and "free" (non-hydrogen-bonded) phenolate A^-, respectively (Table S1). The parameters a and b, assembled in Table S3, are fitting parameters related to the "asymmetry" and "steepness" of the correlation function.

We find that eq 5 is well fulfilled in all cases of the single UV–vis band systems $A2HX^-$ and $A3HX^-$, independent of the different chemical structure and the solvent, CD_2Cl_2 or CDF_3/CDF_2Cl. A satisfactory correlation is also found for $A1HX^-$ in CD_2Cl_2 as illustrated by the dashed line. Because of the larger π-electron system, however, the correlation is shifted as a whole by about 1000 cm^{-1} to the red (see Table S3). The red-shift is found to be somewhat smaller for CDF_3/CDF_2Cl as solvent. This is in agreement with previous findings that λ_{max} of $A1^-$ depends strongly on the environment.[6,38] Thus, the UV–vis absorption of the $A1^-$ moiety is quite susceptible to specific solute–solvent interactions which need to be estimated independently when information about the H-bond geometries is derived from UV–vis absorption frequencies of $A1HX^-$.

After having estimated the hydrogen transfer coordinates of the single UV–vis bands systems we analyzed in the next step the dual band systems of $A2HX^-$ and of $A3HX^-$, exhibiting a proton tautomerism between two forms (Scheme 4b). The relative integrated intensities of the blue bands are included in Table S1 in the column labeled as x_{blue}, from which estimates of the equilibrium constants of tautomerism, $K \approx (1 - x_{blue})/x_{blue}$ can be obtained, assuming that the extinction coefficients of both bands are equal. We proceeded as follows. Using eq 5, we converted the wavenumbers of the blue and the red bands, $\tilde{\nu}_{blue}$ and $\tilde{\nu}_{red}$ to values of q_1 which are then located perfectly on the correlation curves in Figure 6b. These data points are symbolized by open symbols.

Unfortunately, in this graph it is difficult to see how the tautomerism changes the proton transfer coordinates q_1. These quantities were, therefore, visualized in Figure 6c, where we have used the average phenolic 1-^{13}C chemical shifts $\delta^*(\underline{A}HX) = \delta(\underline{A}HX) - \delta(\underline{A}HA)$ to separate the data points. From the top to the bottom, the equilibrium constants K of tautomerism increase in a systematic way. The single data points correspond to $K = 0$ and infinite in the upper left and lower right corner, respectively. For the first data point of type IIa/b we estimate an equilibrium constant of 0.25, whereas the lowest data point of IVa/b exhibits a value of about 5.

The changes of the hydrogen bond geometries in the case of proton tautomerism are visualized in the q_2 vs q_1 correlation plot depicted in Figure 7a. The solid curve refers to equilibrium geometries whereas the dotted curve includes an empirical correction for anharmonic zero-point vibrations as described previously.[28] For the sake of clarity only three types of tautomeric equilibria in Scheme 4b are visualized, typical for IIa/b, IIIa/b, and IVa/b. We note that in the dominant tautomers of IIa and IVb the proton is always further away from the H-bond center as compared to the nondominant tautomers. As the hydrogen bond length q_2 is decreased when H approaches the hydrogen bond center, it follows that the formation of the nondominant tautomer always shortens the hydrogen bond.

^{13}C NMR Chemical Shifts and Hydrogen Bond Geometries. As in OHN hydrogen bonds the nitrogen chemical shift is an excellent probe for the hydrogen–nitrogen distances, the question arose whether and how ^{13}C NMR chemical shifts of AHX^- can be used for a similar purpose. Indeed, recently we had found a monotonous downfield shift of the phenolic carbon in position 1 of $A3HX^-$ when the phenolic oxygen–hydrogen distance is increased.[2] However, the chemical shifts of different phenolic residues do not depend only on the hydrogen bond geometry but also on the type of substituents. We found now that this problem can be solved by referencing the carbon-1 chemical shift of the heteroconjugated anion to the corresponding shift of the homoconjugated anion, usually also present in the solutions studied, i.e. by analyzing the rereferenced chemical shifts δ^* as defined in eq 1. As a demonstration, we have plotted in Figure 7b the ^1H chemical shifts $\delta(A\underline{H}X)$ of $A2HX^-$ and $A3HX^-$ in CD_2Cl_2 and CDF_3/CDF_2Cl as a function of $\delta^*(\underline{A}HX)$. An excellent bell-shaped correlation for the more than 50 data points is obtained which

dx.doi.org/10.1021/ja400611x | J. Am. Chem. Soc. 2013, 135, 7553–7566

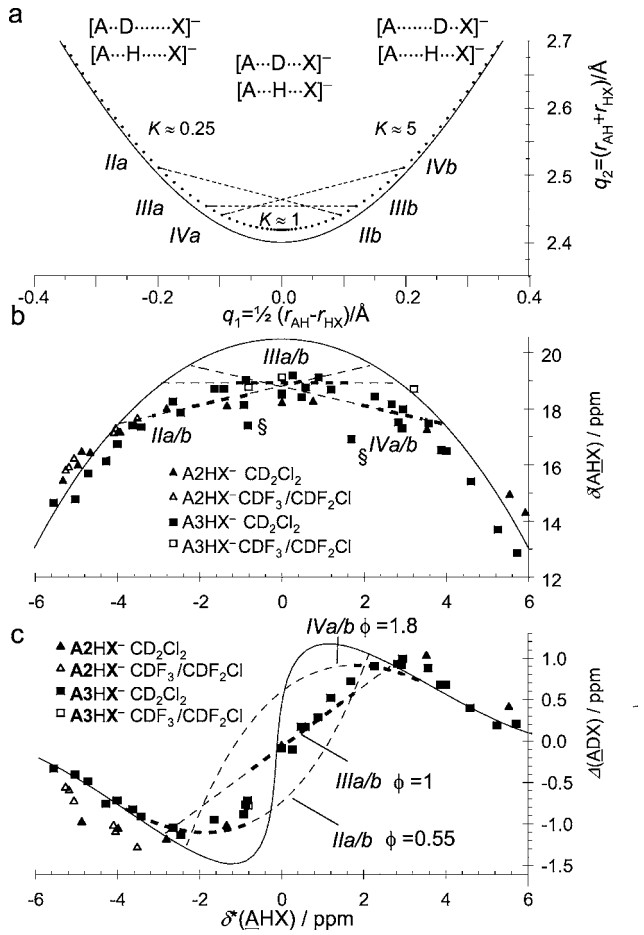

Figure 7. (a) Geometric hydrogen bond correlation between the heavy atom coordinate q_2 and the proton coordinate q_1 according to ref 28. The solid line represents equilibrium geometries and the dotted line an empirical correction for the anharmonicity of hydrogenic zero-point vibrations. The dashed lines represent proton transfer equilibria according to Scheme 4. (b) Correlation between the ^{1}H chemical shifts δ(AHX) of the bridging protons and of the ^{13}C chemical shifts δ^*(AHX). (c) H/D isotope effects on the ^{13}C chemical shifts, Δ(ADX) = δ(ADX) − δ(AHX), as a function of δ^*(AHX). The solid and dashed correlation curves were obtained as described in the text.

is symmetric within the margin of error with respect to the origin of the x-axis. This purely experimental finding indicates indeed that the carbon chemical shifts constitute a convenient measure for the phenolic oxygen−hydrogen distances.

The solid line in Figure 7b was calculated using eq 4 and a more complex expression for the dependence of δ^*(AHX) as a function of q_1, which depended on the chemical shift parameters δ(AH)° = −9 ppm and δ(A)° = 9 ppm of the fictive free AH and A⁻ anion. Details of the calculation have been described recently for OHN hydrogen bonds[39] and in the Supporting Information. The latter contains also additional parameters used to describe the solid line in Figure 7b, valid for equilibrium structures. Whereas the solid line describes well the data of the longer hydrogen bonds in the right and left wings of the graph, the experimental ^{1}H chemical shifts of the stronger hydrogen bonds around δ^*(AHX) = 0 are smaller than the expected value of 20.5 ppm. The maximum value reached is only 19 ppm.

This deviation can be explained in terms of the tautomerism of Scheme 4b discussed above as illustrated by the dashed lines calculated for the asymmetric equilibria of type IIa/b and IVa/b and for the quasi-symmetric equilibrium IIIa/b defined by the dashed lines in Figure 7b. In each situation, the average ^{1}H and ^{13}C chemical shifts depend on the equilibrium constant K and on the limiting chemical shift values defined by the crossing points between the dashed and solid lines. IIa/b describes the experimental data well in the left wing, IIIa/b in the center, and IVa/b in the right wing. The regions where the different equilibria dominate are symbolized by thicker dashed lines. We note that in these regions the experimental data are well reproduced.

In practice, a broad distribution of tautomeric equilibrium constants as illustrated in Scheme 4b needs to be taken into account. Thus, we conclude that the deviation of the solid line in Figure 7b from the dashed line represents a tool to detect a double well situation. In the case of strong intramolecular OHO hydrogen bonds, Perrin et al.,[40] using the NMR isotopic perturbation method, have also found a double well situation.

As compared to the other data points, the two data points in Figure 7b labeled by the symbol "§" indicate significantly lower ^{1}H chemical shifts. They correspond to species A3HX⁻ where X⁻ correspond to the sterically hindered acceptors 2,6-dichloro- and 2,4,6-trichlorophenolate, respectively. This finding indicates that sterically hindered acceptors involve larger O···O distances for quasi-symmetric double wells. For a quantitative interpretation further studies will be necessary.

H/D Isotope Effects. Interesting information about properties of intramolecular hydrogen bonds has been obtained from "secondary" H/D isotope effects on the chemical shifts of neighboring nuclei, in particular of ^{13}C and ^{15}N atoms, e.g., in the residue A[26,32,40,41]

$$\Delta(\underline{A}DX) = \delta(\underline{A}DX) - \delta(\underline{A}HX) \quad (6)$$

Some of us have shown that similar data are also valuable in the case of intermolecular hydrogen bonds, for example those formed by carboxylic acids.[27,32−34] Such isotope effects can have different origins.

"Intrinsic" H/D isotope effects on chemical shifts arise from changes of the hydrogen bond geometries after isotopic substitution, caused by the anharmonicity of hydrogenic ground state vibrations. Geometric isotope effects have been studied and discussed previously for a number of hydrogen bonds.[42,26−28] As illustrated in Figure 7a, when H is far from the hydrogen bond center, deuteration leads to a shortening of the short and a lengthening of the long heavy atom-hydrogen bonds. When H is in the hydrogen bond center, isotope effects are small; a shortening of the A···X distance can occur upon deuteration as D may be more confined in the hydrogen bond center.

"Equilibrium" isotope effects arise from changes of the zero-point energies in the different tautomeric states, leading to different equilibrium constants of tautomerism for the protonated and the deuterated system, K^H and K^D, where $\phi = K^D/K^H$ is called the "fractionation factor". It has been shown that zero-point energies drop along the hydrogen bond correlation in Figure 7a when H is transferred into the hydrogen bond center.[43]

A third possibility is "equilibrium averaged" intrinsic isotope effects even in the absence of isotopic fractionation between two tautomeric states exhibiting, however, different intrinsic isotope effects.[44] The different contributions to the hydrogen bond isotope effects are difficult to separate. In the following,

dx.doi.org/10.1021/ja400611x | J. Am. Chem. Soc. 2013, 135, 7553−7566

we show that this can be done in the cases of AHX^- using UVNMR.

The experimental H/D isotope effects $\Delta(\underline{A}DX)$ on the ^{13}C chemical shifts of the phenolic carbon 1 are plotted in Figure 7c as a function of the ^{13}C chemical shifts $\delta^*(\underline{A}HX)$. The data were derived from the spectra in Figures 2 and 3 as well as from data published previously.[2] We observe an interesting dispersion-like correlation. When H is located near A the isotope effect $\Delta(\underline{A}DX)$ is negative. Its absolute value increases and then drops to zero when the quasi-symmetric configuration at $\delta^*(\underline{A}HX) = 0$ is reached. In this region, signals of $\underline{A}HX^-$ and of $\underline{A}DX^-$ are difficult to resolve as the isotope effects are small. Finally, $\Delta(\underline{A}DX)$ becomes positive, reaches a maximum, and eventually vanishes when H is located near X. As $\delta^*(\underline{A}HX)$ is a measure of the A···H distance, these isotope effects are qualitatively in agreement with the expected intrinsic geometric isotope effects.

However, as was illustrated in Figure 7a and discussed above, in the case of a tautomerism between two asymmetric forms the dominant form exhibits a weaker hydrogen bond as compared to the nondominant form, which implies a loss of zero-point energy in the latter form. Thus, D enriches in the dominant and H in the nondominant form. For the equilibrium IIa/b in Figure 7a, $\phi = K^D/K^H$ is then smaller than 1, and for IVa/b greater than 1, whereas it is close to 1 for IIIa/b.

Using a formalism described previously[28] we have calculated the solid line in Figure 7c which provides a qualitative estimate for the intrinsic isotope effects. The parameters used are described in the Supporting Information. The dashed lines in Figure 7c were calculated for the three types of equilibria using the fractionation factors indicated, taking into account the intrinsic isotope effects at the starting and the ending point. As discussed above in the case of Figure 7b, equilibrium IIa/b dominates when H is close to A and IVa/b when H is close to X, whereas IIIa/b dominates in the case of the quasi-symmetric forms. The regions where the different equilibria dominate are symbolized by thicker dashed lines. We note that in these regions the experimental data are well reproduced. For a more quantitative description, the whole distribution of equilibria should be taken into account which is beyond the scope of this study.

We conclude that the observed equilibrium isotope effects on the carbon chemical shifts can be qualitatively decomposed into the different contributions with the help of UVNMR which can distinguish single-well and dual-well hydrogen bonds to which geometries can be associated via ^1H NMR spectroscopy.

Effects of the Medium Polarity on the Hydrogen Bond Geometries of AHX^-. It is well-known for hydrogen-bonded complexes with zero net charge, such as those formed by a carboxylic acid or a phenol with a nitrogen base, that an increase of the solvent polarity leads to a shift of the bridging proton toward the base, that is, toward the more polar zwitterionic structure.[45] In that case proton transfer is driven by solvation of the polar structure by the polar solvent. This effect has been exploited for example in a recently published study of hydrogen-bonded complexes of acetic acid with pyridines where the temperature dependence of the solvent polarity provided a convenient way of displacing protons in hydrogen bonds and of exploring their pathways by ^1H and ^{13}C NMR.[33] However, conclusions derived for uncharged complexes may not directly be applicable to the charged species presently under investigation, as in the current cases, there is no obvious relationship between proton transfer and changes in solvation energy.

In order to elucidate the solvent influence in the cases of AHX^-, where AH are phenols and HX carboxylic acids let us summarize our observations presented above. In the case of aliphatic carboxylic acids a decrease in the polarity of the medium, realized by a change from CDF_3/CDF_2Cl to CD_2Cl_2, shifts the proton toward the carboxylic group, independently of the initial proton configuration. This effect becomes very small when aliphatic acids are replaced by benzoic acids. Finally, in the case of heteroconjugated phenol-chloride and carboxylic acid-chloride anions a decrease in the solvent polarity leads to proton transfer toward chloride.

All these findings can readily be explained by a concept in which a polar solvent solvates species with localized charges more efficiently than species with more delocalized charges. In this localized charge solvation concept (LCS) an increase in the solvent polarity induces proton transfer in the sense that charge is transferred toward the acceptor less capable of charge delocalization. The latter capability decreases in the order of phenolate, benzoate, aliphatic carboxylate to chloride. The essence of LCS is visualized schematically in Figure 8. In an

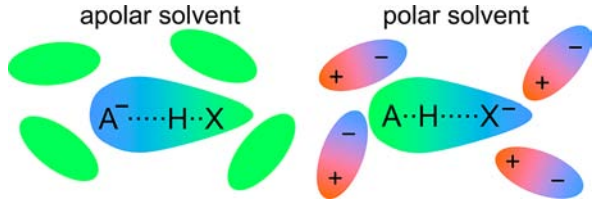

Figure 8. Schematic representation of solvation effects on hydrogen bond geometry in heteroconjugated anions. Polar environments drive proton transfer in the sense that charge becomes more localized.

apolar medium (left), the electrical charge in the asymmetric complex AHX^- is located on the large acceptor A^- offering extended charge delocalization. However, in the polar medium (right), the bridging proton is transferred toward A^- such that charge shifts toward the small acceptor X^- where the electrical charge becomes more localized and hence a more effective interaction with the solvent dipoles can be obtained, increasing solvation energy of the complex as a whole.

Comparison of Solvation Effects in Aprotic and Protic Media. Solvation effects on acid base interaction in protic solvents are very well-known.[46] In dilute solutions, in protic media such as water, acids and bases do not exhibit direct interactions in hydrogen-bonded complexes but are generally dissociated, involving proton transfer to and from the solvent. Hence, solvation effects strongly influence the dissociation equilibria, i.e., the pK_a values. In the case of neutral acid–base complexes, it has been often observed that acids have to be stronger in aprotic environment in order to obtain quasi-symmetric configurations of hydrogen bonds of the type AHB than in water, where weaker acids AH match the pK_a values of the protonated bases.[22,47,48]

In order to compare the acidities of the different proton donors we have plotted in Figure 9 the ^{13}C chemical shifts $\delta^*(\underline{A}HX)$ of the 1-^{13}C carbons of the phenolic fragments obtained for aprotic media as a function of the acidity difference in aqueous solution, $\Delta pK_a = pK_a(HX) - pK_a(AH)$. The open and solid symbols represent phenol–phenolate and the solid symbols stand for phenol-carboxylate and phenolate-carboxylic acid anions. For each series we observed an excellent

dx.doi.org/10.1021/ja400611x | J. Am. Chem. Soc. 2013, 135, 7553–7566

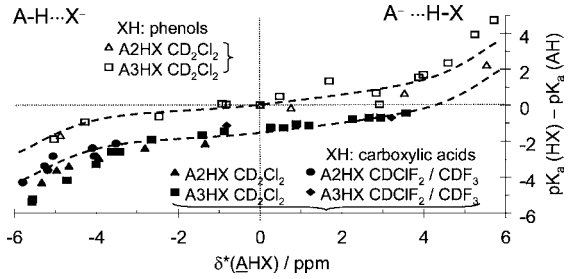

Figure 9. Correlation between the ^{13}C chemical shifts $\delta^*(\underline{A}HX)$ of the complexes AHX^- in CD_2Cl_2 and CDF_3/CDF_2Cl as a function of the pK_a difference of AH and HX in aqueous solution. For further explanation see text.

correlation as illustrated by the dashed sigmoidal lines which serve as guide for the eyes. While the correlation for phenol–phenolate complexes necessarily passes the origin of the graph, the correlation for phenol carboxylate complexes exhibits a vertical offset of more than one pK_a unit. Thus, in order to produce a quasi-symmetric complex in an aprotic solvent a carboxylic acid is needed which is more acidic toward phenolate as compared to aqueous solution. In other words, if a separate carboxylate and phenol are transferred from aqueous solution to a nonaqueous environment the phenol becomes more acidic and the carboxylate more basic. The microscopic explanation is analogous to what was said above with respect to preferential solvation of large and small acceptors in heteroconjugated anions: water preferentially promotes the dissociation of the carboxylic acid over the phenol as the carboxylate is more strongly solvated.

Implications for Photoactive Yellow Protein. In the Introduction we have proposed that the heteroconjugated anions of 4-coumaric acid thioester with carboxylates $A1HX^-$ studied in this work may be regarded as simple models for an isolated hydrogen bond between cofactor and Glu46 in PYP. We find that the bridging protons are located always nearer to the oxygen of A1 rather than of X, giving rise to absorption bands of A1H exhibiting maxima between 373 and 354 nm. From the proton chemical shifts we estimate[28] hydrogen bond OHO distances between 2.50 and 2.53 Å. In environments which are more polar or less polar than our range of media with ε = 18 to 30 we expect shifts of the bridging proton toward the phenolic or carboxylic oxygen atoms, respectively. Due to the low solubility of our model systems in apolar solvents, it remains an open question to what extent such media would induce proton transfer toward the carboxylic group in species of the $A1HX^-$ type.

For the single OHO hydrogen bond between the cofactor model and carboxylates we find here that the proton is located close to the phenolic residue, in contrast to the electronic ground state of the photoactive yellow protein where the phenolic residue carries a negative charge as mentioned in the introduction.[8,11,12,16] Our cofactor model can, however, reproduce the situation in the mutant Tyr42Phe where the hydrogen bond between the cofactor and Tyr42 is replaced by a much longer bond to the aliphatic hydroxyl group of threonine. As a consequence, the H-bond between the cofactor and Glu46 is the only remaining short hydrogen bond.[20] This mutant exists in two forms characterized by their UV–vis spectra: the "yellow form" λ_{max} = 458 nm and the "intermediate spectral form" (λ_{max} = 391 nm).[14,20,49] Preference for either form may be obtained in aqueous solution by addition of chaotropes and kosmotropes, respectively. Joshi et al.[50] concluded from a FTIR spectroscopic study of this mutant that in the intermediate spectral form the side chain of Glu46 is deprotonated. We find the same situation in our small molecule models $A1HX^-$: the deprotonated carboxylate forms a short hydrogen bond to the chromophore which hence gives rise to an absorption band at a wavelength intermediate to free protonated and deprotonated species. Intermediate spectral forms have also been encountered in Tyr42Ala and Tyr42Trp mutants. This suggests that the stabilization of negative charge on the cofactor is related to the formation of the short hydrogen bond between cofactor and Tyr42.

■ CONCLUSIONS

We draw the following conclusions from this work.

(1) A correlation of UV–vis absorption bands of phenols AH in heteroconjugated anions AHX^- with the OH distance has been observed, which is also applicable to the coumarin cofactor in the photoactive yellow protein. In the latter, however, specific intermolecular interactions need to be considered when drawing conclusions about hydrogen bond geometries only by UV spectroscopy.

(2) Using UVNMR it is possible to clearly distinguish between proton transfer pathways involving only no- or low-barrier hydrogen bonds and pathways involving tautomeric equilibria according to Scheme 4, as well as to estimate the geometries of the different structures. The tautomerism pathway is realized in heteroconjugated hydrogen-bonded anions of phenols and carboxylic acids. Perhaps a similar situation is likely to occur for tyrosine-aspartic acid or glutamic acid hydrogen bonds in proteins.

(3) In heteroconjugated anions AHX^- the interplay between charge delocalization and solvation determines the dominant proton position. As illustrated in Figure 8, nonpolar environments favor the charge in the acid residue exhibiting the larger charge delocalization as is the case in phenolates, and polar environments in the residue where the charge is more localized, e.g. in aliphatic carboxylates. Thus, whereas in water phenol is protonated and carboxylic acids deprotonated, in a less polar environment the acidity of the phenol increases relative to that of the carboxylic acid. This result explains the chromophore red shifts of the coumarin cofactor in the protein in terms of slight displacements of the proton across the hydrogen bond center toward a carboxylic group. However, as no dissociation takes place with proton transfer to water, it is not a pK_a shift of the phenolic residue in the enzyme.

(4) Using UVNMR, it has been shown that the ^{13}C chemical shifts of the phenolic 1-^{13}C positions are correlated with the hydrogen bond geometries. Moreover, H/D isotope effects on the ^{13}C chemical shifts could be analyzed and decomposed into intrinsic effects, equilibrium averaged intrinsic effects, and isotopic fractionation between tautomeric states. It is also observed that the nondominant tautomer always exhibits the stronger hydrogen bond as compared to the dominant tautomer.

■ ASSOCIATED CONTENT

Supporting Information

Details of syntheses, additional ^1H, ^{13}C NMR, and normalized UV–vis absorption spectra of heteroconjugated anions of phenols with carboxylic acids, a short description of the hydrogen bond correlation analysis used. Tables: ^1H, ^{13}C NMR, UV–vis parameters of all homo- and heteroconjugated

dx.doi.org/10.1021/ja400611x | J. Am. Chem. Soc. 2013, 135, 7553–7566

anions studied, parameters of the hydrogen bond correlation analyses, pK_a values of all proton donors in water. This material is available free of charge via the Internet at http://pubs.acs.org.

AUTHOR INFORMATION

Corresponding Author

peter.tolstoy@spbu.ru; limbach@chemie.fu-berlin.de

Notes

The authors declare no competing financial interest.

ACKNOWLEDGMENTS

We thank the Deutsche Forschungsgemeinschaft, Bonn (Li 300/29-1) and the Russian Foundation of Basic Research (grant 11-03-00237) for financial support.

REFERENCES

(1) Tolstoy, P. M.; Koeppe, B.; Denisov, G. S.; Limbach, H. H. *Angew. Chem., Int. Ed.* **2009**, *48*, 5745−5747.

(2) Koeppe, B.; Tolstoy, P. M.; Limbach, H.-H. *J. Am. Chem. Soc.* **2011**, *133*, 7897−7908.

(3) Bower, V. E.; Robinson, R. A. *J. Phys. Chem.* **1960**, *64*, 1078−1079.

(4) Hodgson, H. H.; Wignall, J. S. *J. Chem. Soc.* **1927**, 2216−2221.

(5) Meyer, T. E.; Yakali, E.; Cusanovich, M. A.; Tollin, G. *Biochemistry* **1987**, *26*, 418−423.

(6) Sprenger, W. W.; Hoff, W. D.; Armitage, J. P.; Hellingwerf, K. J. *J. Bacteriol.* **1993**, *175*, 3096−3104.

(7) Baca, M.; Borgstahl, G. E. O.; Boissinot, M.; Burke, P. M.; Williams, D. R.; Slater, K. A.; Getzoff, E. D. *Biochemistry* **1994**, *33*, 14369−14377.

(8) Borgstahl, G. E. O.; Williams, D. R.; Getzoff, E. D. *Biochemistry* **1995**, *34*, 6278−6287.

(9) Yamaguchi, S.; Kamikubo, H.; Kurihara, K.; Kuroki, R.; Niimura, N.; Shimizu, N.; Yamazaki, Y.; Kataoka, M. *Proc. Natl. Acad. Sci. U.S.A.* **2009**, *106*, 440−444.

(10) Sigala, P. A.; Tsuchida, M. A.; Herschlag, D. *Proc. Natl. Acad. Sci. U.S.A.* **2010**, *106*, 9232−9237.

(11) Meyer, T. E. *Biochim. Biophys. Acta* **1985**, *806*, 175−183.

(12) Kim, M.; Mathies, R. A.; Hoff, W. D.; Hellingwerf, K. J. *Biochemistry* **1995**, *34*, 12669−12672.

(13) Xie, A.; Hoff, W. D.; Kroon, A. R.; Hellingwerf, K. J. *Biochemistry* **1996**, *35*, 14671−14678.

(14) Kroon, A. R.; Hoff, W. D.; Fennema, H. P. M.; Gijzen, J.; Koomen, G.-J.; Verhoeven, J. W.; Crielaard, W.; Hellingwerf, K. J. *J. Biol. Chem.* **1996**, *271*, 31949−31956.

(15) Dawson, R. M. C.; Elliot, D. C.; Elliot, W. H.; Jones, K. M. *Data for Biochemical Research*; Oxford Science Publications: Oxford, 1986.

(16) Demchuk, E.; Genick, U. K.; Woo, T. T.; Getzoff, E. D.; Bashford, D. *Biochemistry* **2000**, *39*, 1100−1113.

(17) Yoda, M.; Inoue, Y.; Sakurai, M. *J. Phys. Chem. B* **2003**, *107*, 14569−14575.

(18) Genick, U. K.; Devanathan, S.; Meyer, T. E.; Canestrelli, I. L.; Williams, E.; Cusanovich, M. A.; Tollin, G.; Getzoff, E. D. *Biochemistry* **1997**, *36*, 8−14.

(19) Hendriks, J.; Hoff, W. D.; Crielaard, W.; Hellingwerf, K. J. *J. Biol. Chem.* **1999**, *274*, 17655−17660.

(20) Brudler, R.; Meyer, T. E.; Genick, U. K.; Devanathan, S.; Woo, T. T.; Millar, D. P.; Gerwert, K.; Cusanovich, M. A.; Tollin, G.; Getzoff, E. D. *Biochemistry* **2000**, *39*, 13478−13486.

(21) Morgan, S. O.; Lowry, H. H. *J. Phys. Chem.* **1930**, *34*, 2385−2432.

(22) Golubev, N. S.; Denisov, G. S.; Smirnov, S. N.; Shchepkin, D. N.; Limbach, H. H. *Z. Phys. Chem.* **1996**, *196*, 73−84.

(23) Shenderovich, I. G.; Burtsev, A. P.; Denisov, G. S.; Golubev, N. S.; Limbach, H. H. *Magn. Reson. Chem.* **2001**, *39*, S91−99.

(24) Sharif, S.; Denisov, G. S.; Toney, M. D.; Limbach, H. H. *J. Am. Chem. Soc.* **2007**, *129*, 6313−6327.

(25) Smirnov, S. N.; Golubev, N. S.; Denisov, G. S.; Benedict, H.; Schah-Mohammedi, P.; Limbach, H. H. *J. Am. Chem. Soc.* **1996**, *118*, 4094−4101.

(26) Limbach, H. H.; Denisov, G. S.; Golubev, N. S. Hydrogen Bond Isotope Effects Studied by NMR. In *Isotope Effects in the Biological and Chemical Sciences*; Kohen, A., Limbach, H. H., Eds.; Taylor & Francis: Boca Raton, FL, 2005; Chapter 7, pp 193−230.

(27) Tolstoy, P. M.; Schah-Mohammedi, P.; Smirnov, S. N.; Golubev, N. S.; Denisov, G. S.; Limbach, H. H. *J. Am. Chem. Soc.* **2004**, *126*, 5621−5634.

(28) Limbach, H. H.; Tolstoy, P. M.; Pérez-Hernández, N.; Guo, J.; Shenderovich, I. G.; Denisov, G. S. *Israel J. Chem.* **2009**, *49*, 199−216.

(29) (a) Sternberg, U.; Brunner, E. *J. Magn. Reson.* **1994**, *108*, 142−150. (b) Harris, T. K.; Zhao, Q.; Mildvan, A. S. *J. Mol. Struct.* **2000**, *552*, 97−109.

(30) Jeffrey, G. A.; Yeon, Y. *Acta Cryst. B* **1986**, *B42*, 410−413.

(31) Gu, Z.; Zambrano, R.; McDermott, A. *J. Am. Chem. Soc.* **1994**, *116*, 6368−6372.

(32) Schah-Mohammedi, P.; Shenderovich, I. G.; Detering, C.; Limbach, H. H.; Tolstoy, P. M.; Smirnov, S. N.; Denisov, G. S.; Golubev, N. S. *J. Am. Chem. Soc.* **2000**, *122*, 12878−12879.

(33) Tolstoy, P.; Guo, J.; Koeppe, B.; Golubev, N.; Denisov, G.; Smirnov, S.; Limbach, H. H. *J. Phys. Chem. A* **2010**, *114*, 10775−10782.

(34) Tolstoy, P. M.; Guo, J.; Koeppe, B.; Golubev, N. S.; Denisov, G. S.; Smirnov, S. N.; Limbach, H. H. *J. Phys. Chem. A* **2012**, *116*, 11370−11387.

(35) Detering, C.; Tolstoy, P. M.; Golubev, N. S.; Denisov, G. S.; Limbach, H. H. *Doklady Phys. Chem.* **2001**, *379*, 1−4.

(36) Brown, H. C.; McDaniel, D. H.; Häfliger, O. In *Determination of Organic Structures by Physical Methods*; Braude, E. A., Nachod, F. C., Eds.; Academic Press: New York, 1955; pp 567−662.

(37) Steiner, Th. *J. Phys. Chem. A* **1998**, *102*, 7041−7052.

(38) Usman, A.; Mohammed, O. F.; Heyne, K.; Dreyer, J.; Nibbering, E. T. J. *Chem. Phys. Lett.* **2005**, *401*, 157−163.

(39) Ip, B. C. K.; Shenderovich, I. G.; Tolstoy, P. M.; Frydel, J.; Denisov, G. S.; Buntkowsky, G.; Limbach, H. H. *J. Phys. Chem. A* **2012**, *116*, 11180−11188.

(40) (a) Perrin, C. L. *Acc. Chem. Res.* **2010**, *43*, 1550−1557. (b) Perrin, C. L.; Karri, P.; Moore, C.; Rheingold, A. L. *J. Am. Chem. Soc.* **2012**, *134*, 7766−7772.

(41) Dziembowska, T.; Hansen, P. E.; Rozwadowski, Z. *Progr. NMR Spect.* **2004**, *45*, 1−29.

(42) Benedict, H.; Limbach, H. H.; Wehlan, M.; Fehlhammer, W. P.; Golubev, N. S.; Janoschek, R. *J. Am. Chem. Soc.* **1998**, *120*, 2939−2950.

(43) Smirnov, S. N.; Benedict, H.; Golubev, N. S.; Denisov, G. S.; Kreevoy, M. M.; Schowen, R. L.; Limbach, H. H. *Can. J. Chem.* **1999**, *77*, 943−949.

(44) Sharif, S.; Denisov, G. S.; Toney, M. D.; Limbach, H. H. *J. Am. Chem. Soc.* **2006**, *128*, 3375−3387.

(45) (a) Bell, C. L.; Barrow, G. M. *J. Chem. Phys.* **1959**, *31*, 1158−1163. (b) Baba, H.; Matsuyama, A.; Kokubun, H. *J. Chem. Phys.* **1964**, *41*, 895−896. (c) Baba, H.; Matsuyama, A.; Kokubun, H. *Spectrochim. Acta* **1969**, *25A*, 1709−1722. (d) Hudson, R. A.; Scott, R. M.; Vinogradov, S. N. *J. Phys. Chem.* **1972**, *76*, 1989−1993. (e) Romanowski, H.; Sobczyk, L. *J. Phys. Chem.* **1975**, *79*, 2535−2542.

(46) Reichardt, C. Solvent Effects on the Position of Homogeneous Chemical Equilibria. In *Solvents and Solvent Effects in Organic Chemistry*, 3rd ed.; Wiley-VCH: Weinheim, Germany, 2003; pp 93−146.

(47) (a) Ratajczak, H.; Sobczyk, L. *J. Chem. Phys.* **1969**, *50*, 556−557. (b) Sobczyk, L.; Pawelka, Z. *J. Chem. Soc. Faraday Trans. I* **1974**, *70*, 832−838.

(48) (a) Pawlak, Z.; Magonski, J.; Jasinski, T. *J. Mol. Struct.* **1978**, *47*, 329−338. (b) Magonski, J.; Pawlak, Z.; Jasinski, T. *J. Mol. Struct.* **1982**, *80*, 243−250.

(49) (a) Mihara, K.; Hisatomi, O.; Imamoto, Y.; Kataoka, M.; Tokunaga, F. *J. Biochem.* **1997**, *121*, 876−880. (b) Imamoto, Y.; Koshimizu, H.; Mihara, K.; Hisatomi, O.; Mizukami, T.; Tsujimoto, K.;

Kataoka, M.; Tokunaga, F. *Biochemistry* **2001**, *40*, 4679−4685. (c) Meyer, T. E.; Devanathan, S.; Woo, T.; Getzoff, E. D.; Tollin, G.; Cusanovich, M. A. *Biochemistry* **2003**, *42*, 3319−3325.
(50) Joshi, C. P.; Otto, H.; Hoersch, D.; Meyer, T. E.; Cusanovich, M. A.; Heyn, M. P. *Biochemistry* **2009**, *48*, 9980−9993.
(51) Jencks, W.; Regenstein, J. In *Handbook of Biochemistry and Molecular Biology*, 3rd ed.; Fasman, G. D., Ed.; CRC Press: Cleveland, 1976; Vol. *1*, pp 305−351.